American Journal of Mathematical and Computer Modelling
2026; 11(1): 67-80
http://www.sciencepublishinggroup.com/j/ajmcm
doi: 10.11648/j.ajmcm.20261101.16

Modeling Extreme Rainfall Events Using Stationary and Non-stationary Peaks-Over-Threshold Frameworks in EVT

Simion Mike Mbumbu*, **Anthony Waititu, Herbert Imboga, Susan Mwelu**

Department of Statistics and Actuarial Sciences, Jomo Kenyatta University of Agriculture and Technology, Juja, Kenya

Email address:
mbumbumike5@gmail.com (Simion, Mike Mbumbu), awaititu@jkuat.ac.ke (Anthony Waititu), imbogaherbert@jkuat.ac.ke (Herbert Imboga), smwelu@jkuat.ac.ke (Susan Mwelu)
*Corresponding author

To cite this article:
Simion Mike Mbumbu, Anthony Waititu, Herbert Imboga, Susan Mwelu. (2026). Modeling Extreme Rainfall Events Using Stationary and Non-stationary Peaks-Over-Threshold Frameworks in EVT. *American Journal of Mathematical and Computer Modelling, 11*(1), 67-80. https://doi.org/10.11648/j.ajmcm.20261101.16

Received: 31 January 2026 ; **Accepted:** 20 February 2026 ; **Published:** 18 March 2026

Abstract: Kenya has in recent years experienced a surge in extreme rainfall events, which continue to pose serious risks to human life, infrastructure, and the wider economy. This study aimed to develop a non-stationary Generalized Pareto Distribution(GPD). Its performance was compared with the classical stationary Peaks-Over-Threshold (POT) model to improve the modeling and prediction of extreme rainfall events. Accurately modeling these extremes is therefore essential to support sound risk assessment and informed decision-making. An Extreme Value Theory(EVT)–based threshold exceedance framework was used to model rainfall extremes, contrasting stationary and non-stationary Generalized Pareto formulations. Under the non-stationary framework, key environmental covariates were incorporated. These included Sea Surface Temperature (SST), Atmospheric Moisture Content (AMC), and Impervious Surface Percentage (ISP). These covariates account for ocean-driven climate variability, atmospheric moisture availability, and land-surface modifications influencing local atmospheric moisture, respectively. The findings indicate that the most suitable model was one in which the shape parameter varied with SST and the scale parameter with AMC. This model yielded lower information criterion values, reflecting a superior fit. This preference was further supported by a likelihood-ratio test, which indicated significance at $p < 0.05$. The model enabled the estimation of return levels and the assessment of rainfall-related risks in Kenya. By accounting for climatic and land-surface drivers, the study offers a stronger basis for risk assessment and delivers guidance for urban planning, policymaking, and strategies for disaster preparedness.

Keywords: Extreme Rainfall, Generalized Pareto Distribution, Peaks-over-threshold, Nonstationary Models, Return Levels

1. Introduction

Rainfall distribution has shifted significantly in recent decades, with some regions experiencing heightened precipitation while others face prolonged dry spells [35]. These changes are largely driven by anthropogenic global warming, which strengthens the hydrological cycle and increases the likelihood of short, intense rainfall events [35]. Daily rainfall variability has increased by approximately 1.2% per decade, leading to more concentrated extreme episodes. In East Africa, including Kenya, these trends have contributed to a higher frequency of extreme rainfall events, posing substantial risks to human life, infrastructure, and agriculture. Understanding and predicting such extremes is critical for effective climate risk assessment and disaster preparedness.

Extreme rainfall is primarily driven by increases in atmospheric moisture amplified by climate change [28]. Warmer sea surface temperatures elevate evaporation and atmospheric moisture, intensifying rainfall events. According to previous work, Africa had the warmest seas in 2024, with sea surface temperatures higher than those observed over other continents [34]. Urbanization and impervious surfaces further exacerbate local warming. These physical drivers form the basis for incorporating nonstationary environmental covariates in statistical models for extreme rainfall.

Severe rainfall events in recent decades have caused substantial global impacts. For example, floods in Europe in 2021 resulted in nearly 243 fatalities [15], Pakistan in 2022 saw over 1400 deaths [6], and in Africa, 2024 floods affected 27 countries, claiming approximately 2,500 lives [3]. In Kenya, torrential rains in April-May 2024 caused a dam burst in Mai Mahiu, killing over 40 people and damaging homes, roads, and farmland [1]. These events highlight the growing risks of extreme rainfall and the need for robust predictive models.

Classical stationary models assume constant parameters, limiting their ability to capture climatic and land-surface variability. Nonstationary frameworks overcome this by allowing parameters to vary with environmental covariates such as Sea Surface Temperature, Atmospheric Moisture Content, and Impervious Surface Percentage [21]. Within the POT framework, the GPD approximates threshold exceedances, and incorporating covariates allows parameters to reflect evolving environmental conditions, improving extreme rainfall estimation [12].

Building on this framework, the present study develops a modified POT approach to incorporate time-varying covariates (SST, AMC and ISP). It evaluates model performance with historical rainfall data, estimates return levels, and generates risk assessments. This approach enhances prediction accuracy and supports evidence-based decision-making in Kenya, where high-impact precipitation events are increasing in frequency and intensity.

2. Literature Review

2.1. Rainfall Variability

Recent studies document significant changes in rainfall characteristics. Zhang et al. reported shifts in precipitation regimes linked to anthropogenic warming [35], while other studies showed that climate change has intensified short-term rainfall variability, increasing flash flood risk and pressure on water management systems [10, 32].

Using a high-resolution global flood model,previous studies projected that global flood hazards could increase by nearly 49% by 2100 under a high-emissions scenario (Shared Socioeconomic Pathway 5-8.5), with substantially smaller increases under low-emission pathways [33]. These findings highlight the importance of accurately characterizing high-intensity rainfall events that drive flooding.

In East Africa, however, long-term rainfall trends are less consistent. Early work reported by previous studies found no persistent long-term trends at many stations, a result later confirmed by further analyses for Ethiopia, Kenya, and Tanzania [30, 16]. While seasonal variations in the long and short rains exist [11], overall annual rainfall trends remain weak. Similar findings in Kenyan catchments such as the Upper Tana Basin suggest that rainfall variability is dominated by inter-annual and seasonal fluctuations rather than monotonic long-term change [26].

Recent studies indicate growing interest in advanced statistical modeling of climate extremes and their impacts in Kenya. For instance, Mulwa et al. developed a hybrid Extreme Value Theory-Copula-XGBoost framework to model compound drought and heatwave extremes in Kenya, demonstrating the relevance of Extreme Value Theory (EVT) in capturing complex tail behavior in climate variables [25].

2.2. Theoretical Foundation of EVT

EVT provides a robust statistical framework to estimate the likelihood of high-impact events and forms the foundation for modeling extreme observations using two main approaches: Block Maxima (BM) and POT. The BM method extracts the maximum observation within predefined intervals and fits them to the Generalized Extreme Value (GEV) distribution [18].

By contrast, the POT method considers exceedances above a selected high threshold and models them with the GPD. Previous studies highlighted the usefulness of EVT for characterizing hydrological extremes, noting that POT methods make fuller use of extreme observations above a high threshold compared to BM approaches [20]. This approach makes fuller use of the available information, capturing a larger set of relevant extreme events. For both BM and POT to produce reliable estimates, assumptions such as stationarity and independence of observations are generally required.

Despite its simplicity, BM has notable drawbacks. It may misclassify ordinary high values as extremes when the maximum within a block does not reflect a genuinely rare event. As observed in previous work, BM often loses valuable information by relying on only one value per block [12]. The POT framework addresses these limitations by focusing directly on threshold exceedances, whether fixed or time-varying. This makes POT a more efficient and flexible approach for studying extremes, particularly rainfall events where accurate representation of intensity and frequency is essential in non-stationary settings.

2.3. The Generalized Pareto Distribution

Within the POT framework, the GPD provides an appropriate approximation for threshold exceedances [29]. Its scale parameter governs exceedance magnitude, while the shape parameter controls tail behavior, ranging from bounded to heavy-tailed extremes [12]. This flexibility makes the GPD well suited for modeling extreme rainfall, which is often characterized by rare but intense events, and enables more reliable estimation of return levels in hydrological applications.

2.4. Application of EVT to Rainfall Analysis

EVT has found extensive use in hydrology and climatology to characterize rainfall extremes and their associated risks. For instance, Acero et al. analyzed daily rainfall data from stations across the Iberian Peninsula using a non-stationary POT approach with a time-varying threshold and declustering to ensure independence. They found spatial and seasonal variations, with decreases in short-return extremes and increases in longer-return extremes, especially during autumn [2]. Similarly, Begueria et al. applied a Poisson-GPD model in northeast Spain, observing weak annual trends but clear seasonal shifts, including declines in winter extremes and higher spring precipitation along Mediterranean coastal areas [9]. Both studies highlight the importance of capturing temporal and seasonal variability when modeling rainfall extremes.

Kyojo et al. and Onwuegbuche et al. applied EVT to analyze high-impact rainfall in East Africa, focusing on Tanzania and Kenya, respectively [22, 27]. Kyojo et al. fitted the GEV distribution to daily rainfall exceedances (1990-2020) and compared L-moments, maximum likelihood estimation (MLE), and Bayesian inference using Markov Chain Monte Carlo (MCMC), finding Bayesian methods yielded superior parameter estimates [22]. Onwuegbuche et al. used both GEV and GPD approaches on historical Kenyan data (1901-2016), showing that the GPD predicted higher rainfall for shorter return periods, while the GEV captured larger extremes for longer periods [27]. Both studies confirmed that EVT provides reliable estimates of return levels and extreme rainfall behavior. Collectively, their findings demonstrate the utility of EVT for preparing for high-impact rainfall events in climate-sensitive East African regions.

2.5. Advances in Non-Stationary EVT Models

According to previous work, relying on stationary models to assess extreme climatic events may lead to underestimations of risk, especially as climate patterns continue to change. This work emphasizes the need to adopt statistical models that allow parameters to vary with time. This makes the models more responsive to observed shifts in extreme rainfall and temperature events. By incorporating non-stationarity into these models, the accuracy of long-term risk predictions can be significantly improved, particularly in the context of climate related hazards [21].

Ghalavand et al. applied non-stationary GEV models to 36 Iranian stations (1960-2021), capturing temporal and spatial rainfall trends. Although Akaike Information Criterion (AIC) did not consistently select non-stationary models, they still outperformed in predictive accuracy (Root Mean Square Error, Nash-Sutcliffe Efficiency) and revealed regional variability driven by local climate factors, supporting covariate-informed approaches [17]. Similarly, Dey and Patwary incorporated dry-bulb temperature in a non-stationary GEV model for Bangladesh (1999-2015), accounting for seasonal shifts and ongoing extremes. In this study, Chattogram showed higher probabilities of extreme rainfall than Dhaka, and uncertainties were evaluated using the delta method and parametric bootstrap, emphasizing the value of covariate-driven non-stationary models for flood risk management and urban planning [13].

2.6. Comparison Between Stationary and Non-Stationary Models

Several studies have emphasized the limitations of stationary extreme value models and the advantages of incorporating non-stationarity. For instance, Roth et al. applied a regional POT framework with time-dependent GPD parameters, showing that nonstationary models captured temporal variability in precipitation extremes more effectively than stationary alternatives and produced more reliable return level estimates under changing climate conditions [31].

Hao et al. compared stationary and non-stationary models in the Hanjiang River Basin, China, analyzing Rx5day and R20 indices using Generalized Additive Models for Location, Scale, and Shape (GAMLSS). Three models were examined: M0 (stationary), M1 (non-stationary with time), and M2 (non-stationary with large-scale climate indices). Results revealed clear non-stationarity across all stations, with M2 outperforming M1, highlighting the importance of incorporating covariates to improve predictions of precipitation extremes [19].

Masingi and Maposa examined monthly precipitation across five South African provinces using stationary and non-stationary GEVs. Rainfall in Limpopo and Mpumalanga exhibited non-stationary behavior, whereas stationary models were adequate for the other provinces, demonstrating the need for flexible modeling strategies under changing climatic conditions [24].

Maposa et al. evaluated non-stationary GEV models for peak floods in Mozambique's lower Limpopo River basin. Location and scale parameters were allowed to change linearly over time and compared with stationary models. Significant trends were found for the scale parameter at some sites, while location trends were largely insignificant, emphasizing the value of extending stationary GEV models to non-stationary frameworks to capture climate-driven shifts in flood behavior [23].

2.7. Summary of Literature Gaps

Despite extensive EVT applications, key gaps remain:

1. Limited use of climatic covariates beyond time in non-stationary models;
2. Sparse coverage of extreme rainfall studies in East Africa, particularly Kenya;
3. Underutilization of modified POT models with covariate-dependent parameters.

This study addresses these gaps by developing a modified POT framework incorporating climatic covariates to better characterize high-impact rainfall events in Kenya.

3. Methodology

3.1. Data Source and Description

Rainfall data used in this study were obtained from TerraClimate (1960-1980) and the Climate Hazards Group

InfraRed Precipitation with Station data (CHIRPS) dataset (1981-2024). The two datasets were combined to create a continuous long-term record for Kenya. SST (1960-2024) was sourced from National Oceanic and Atmospheric Administration (NOAA), with variations, particularly through El Niño-Southern Oscillation (ENSO) events, influencing East African rainfall patterns. The second covariate, AMC (1960-2024) from the ECMWF Reanalysis 5th Generation (ERA5) dataset, reflects the amount of water vapor available in the atmosphere. ISP, calculated using the Global Human Settlement Layer (GHSL) in Quantum Geographic Information System (QGIS), serves as a proxy for land-use change and human influence. These covariates are represented as z_1 (SST), z_2 (AMC), and z_3 (ISP). All statistical analyses were performed using R software.

3.2. Data Aggregation and Scale

The study used rainfall data aggregated to the national level, which provides a coherent characterization of extreme rainfall behavior in Kenya. This aggregation establishes a baseline tail behavior and a reference non-stationary structure for future region-specific analyses. This national level study also provides an opportunity for cross country comparison. It provides insights for future extreme rainfall behavior comparison across East Africa or even Africa, where Kenya serves as a coherent unit of analysis within the broader context. National-scale aggregation supports risk assessment by disaster agencies and other stakeholders, aligning with the scale at which climate adaptation and disaster preparedness planning is typically coordinated. From a physical perspective, the approach is consistent with large-scale climatic drivers, particularly sea surface temperature, incorporated in the non-stationary framework.

At the same time, aggregation smooths localized, high-intensity events, which can reduce variability in extremes and lead to more stable return level estimates. While this is beneficial for national-scale risk assessment and model comparison, it may underestimate site-specific extremes, making the estimates more suitable for strategic planning rather than local engineering design. Importantly, because both stationary and non-stationary POT models are fitted to the same aggregated data, comparisons between models remain valid despite spatial averaging.

3.3. Data Preprocessing

The GHSL dataset provided data from 1975–2024; values for 1960–1974 were estimated using a logistic or linear model, with the best-fitting model selected via AIC. CHIRPS reliability has been widely validated across Africa. It demonstrates strong performance in capturing monthly rainfall and reproducing spatial patterns in complex topography. The dataset also supports water resource planning, especially when calibrated with local observations [4, 5, 7, 14].

TerraClimate (1960–1980) and CHIRPS (1981–2024) were combined using the stitching method. Compatibility over the overlap period (1981–2024) was confirmed using normality tests, correlation analysis, graphical procedures, and Kolmogorov–Smirnov(KS) tests. Data distributions and temporal patterns were examined to guide threshold selection and covariate analysis. Trends in rainfall and covariates were evaluated using the Mann–Kendall (MK) test for both annual and seasonal series (long rains: March–May(MAM); short rains: October–December(OND)), providing insight into potential climate-driven changes.

3.4. The Generalized Pareto Distribution

The Pickands–Balkema–de Haan theorem [8, 29] states that, for a sufficiently high threshold, excesses over that threshold converge to a GPD. This underpins the POT method in EVT, providing a flexible framework to model the tail behavior of rainfall, particularly under non-stationary climate conditions.

EVT assumes that exceedances are independent and identically distributed (i.i.d.) and that the underlying process is stationary [12]. Stationarity implies that key statistical features (mean and variance) remain constant over time, while i.i.d. ensures that each extreme event is drawn from the same probability law and occurs independently.

For rainfall observations R_t and a threshold u, exceedances are defined as:

$$y_t = R_t - u, \quad \text{for all } R_t > u,$$

where $y_t \geq 0$. The GPD describing these exceedances is given by

$$f(y_t; \xi, \sigma) = \begin{cases} \frac{1}{\sigma}\left(1 + \xi \frac{y_t}{\sigma}\right)^{-1/\xi - 1}, & \xi \neq 0, \\ \frac{1}{\sigma}\exp\left(-\frac{y_t}{\sigma}\right), & \xi = 0, \end{cases} \tag{1}$$

with cumulative distribution function (CDF)

$$F(y_t; \xi, \sigma) = \begin{cases} 1 - \left(1 + \xi \frac{y_t}{\sigma}\right)^{-1/\xi}, & \xi \neq 0, \\ 1 - \exp\left(-\frac{y_t}{\sigma}\right), & \xi = 0, \end{cases} \tag{2}$$

where $\sigma (> 0)$ is the scale parameter and ξ is the shape parameter. Positive ξ indicates heavy tails, $\xi \approx 0$ corresponds to an exponential tail, and negative ξ implies an upper bound on extremes.

3.5. Stationary GPD Model

3.5.1. Threshold Selection

Extreme rainfall events were defined as exceedances over candidate quantiles (0.90–0.95) of the rainfall distribution. The stability of the shape parameter ξ across thresholds and adherence of Quantile-Quantile (Q-Q) and Probability-Probability (P-P) plots to the diagonal line guided the selection. Thresholds above the 95th percentile were avoided due to insufficient exceedances.

3.5.2. Parameter Estimation

Parameters of the stationary GPD were estimated using Maximum Likelihood Estimation (MLE). Let $y_1, \ldots, y_n$

denote exceedances over threshold u. The log-likelihood function is

$$\ell(\sigma,\xi) = -n\log\sigma - \left(\frac{1}{\xi}+1\right)\sum_{t=1}^{n}\log\left(1+\xi\frac{y_t}{\sigma}\right), \quad \xi \neq 0. \tag{3}$$

For $\xi = 0$, the GPD simplifies to the exponential distribution, and the estimation proceeds similarly.

3.6. Non-Stationary GPD Model

3.6.1. Threshold Selection

Rainfall data were first examined using a time series plot to assess the suitability of a fixed threshold. This visual assessment was complemented by the MK test to detect the presence of any long-term trend in extreme rainfall. The presence of a significant trend would motivate the use of a time-varying threshold, estimated using quantile regression; otherwise, a constant threshold would be adopted. For the time-varying threshold, the quantile regression model would incorporate the climate-related covariates, reflecting their influence on rainfall extremes.

The evaluation presented in Chapter 4 showed no significant trend in the data, indicating that a constant threshold was sufficient for this study. The time-varying threshold approach is therefore included to document the methodological considerations and to illustrate alternative threshold selection strategies, rather than as part of the final applied analysis.

3.6.2. Non-Stationary Model Specification

The non-stationary GPD was constructed using the threshold identified earlier. In this model, the scale and shape parameters are functions of the covariates $\mathbf{z}_t = (z_{1,t}, z_{2,t}, z_{3,t})$:

$$\sigma(\mathbf{z}_t) = \exp(\beta_0 + \beta_1 z_{1,t} + \beta_2 z_{2,t} + \beta_3 z_{3,t}), \tag{4}$$

$$\xi(\mathbf{z}_t) = \gamma_0 + \gamma_1 z_{1,t} + \gamma_2 z_{2,t} + \gamma_3 z_{3,t} \tag{5}$$

The exponential form for $\sigma(\mathbf{z}_t)$ ensures positivity and allows flexible modeling. The resulting non-stationary GPD has Probability Density Function (PDF):

$$f(y_t \mid \sigma(\mathbf{z}_t), \xi(\mathbf{z}_t)) = \tag{6}$$

$$\begin{cases} \dfrac{1}{\sigma(\mathbf{z}_t)}\left(1+\dfrac{\xi(\mathbf{z}_t)\,y_t}{\sigma(\mathbf{z}_t)}\right)^{-1/\xi(\mathbf{z}_t)-1}, & \xi(\mathbf{z}_t)\neq 0, \\ \dfrac{1}{\sigma(\mathbf{z}_t)}\exp\left(-\dfrac{y_t}{\sigma(\mathbf{z}_t)}\right), & \xi(\mathbf{z}_t)=0. \end{cases}$$

and CDF:

$$F(y_t \mid \sigma(\mathbf{z}_t), \xi(\mathbf{z}_t)) = \tag{7}$$

$$\begin{cases} 1-\left(1+\dfrac{\xi(\mathbf{z}_t)\,y_t}{\sigma(\mathbf{z}_t)}\right)^{-1/\xi(\mathbf{z}_t)}, & \xi(\mathbf{z}_t)\neq 0, \\ 1-\exp\left(-\dfrac{y_t}{\sigma(\mathbf{z}_t)}\right), & \xi(\mathbf{z}_t)=0. \end{cases}$$

The non-stationary GPD was then fitted to exceedances over the threshold with scale and shape parameters varying with the selected covariates.

3.6.3. Parameter Estimation

MLE was used to estimate the scale and shape parameters of the non-stationary GPD, incorporating covariate effects. Let $y_1, \ldots, y_n$ be the exceedances and $\sigma_t = \sigma(\mathbf{z}_t)$, $\xi_t = \xi(\mathbf{z}_t)$ the covariate-dependent parameters. The log-likelihood function is

$$\ell(\theta) = \sum_{t=1}^{n}\log f(y_t \mid \sigma_t, \xi_t), \tag{8}$$

where $f(y_t \mid \sigma_t, \xi_t)$ is the non-stationary GPD PDF. Covariates were standardized prior to fitting to facilitate convergence. The resulting MLEs provide estimates of the covariate-dependent scale and shape parameters for the non-stationary GPD.

3.7. Model Fit Assessment

The adequacy of the stationary and non-stationary GPD models was evaluated using standard diagnostics:

1. *P-P Plot:* Empirical probabilities of exceedances were plotted against theoretical probabilities from the fitted model. Close adherence to the diagonal supports model adequacy.
2. *Q-Q Plot:* Empirical quantiles were compared to model-based quantiles. Close adherence to the diagonal supports model adequacy.
3. *Kolmogorov-Smirnov Test:* The KS test was used to statistically compare the empirical and theoretical cumulative distribution functions (CDFs). For non-stationary models, the CDF varies with covariates and was evaluated accordingly.

3.8. Model Comparison and Evaluation

Model performance was assessed to determine whether the stationary or non-stationary GPD better captures extreme rainfall. The Akaike Information Criterion (AIC) and Bayesian Information Criterion (BIC) were used to evaluate fit while penalizing model complexity, with lower values indicating more efficient models. Additionally, a Likelihood Ratio Test (LRT) tested whether including covariates significantly improved the fit over the stationary model. This multi-criteria approach ensured the selected model balances accuracy, interpretability, and predictive performance.

3.9. Estimate Return Levels

Return levels and associated risk estimates were computed using the best-performing GPD model. Return levels provide essential information for flood risk assessment and climate adaptation planning. For the non-stationary GPD, return levels were derived as the mean across all conditional estimates, reflecting typical environmental conditions. The return level y_T for a return period T is given by:

$$y_T = u + \frac{\sigma}{\xi}\left[(T \cdot \lambda_u)^{\xi} - 1\right], \quad \xi \neq 0 \tag{9}$$

$$y_T = u + \sigma \ln(T \cdot \lambda_u), \quad \xi = 0 \tag{10}$$

where:

1. u is the threshold,
2. σ is the scale parameter,
3. ξ is the shape parameter,
4. λ_u is the rate of exceedances above u.

The probability of exceedance above the threshold u is:

$$P(R_t > u) \approx \frac{1}{n}\sum_{i=1}^{n} \mathbb{I}(R_t > u), \quad \mathbb{I}(R_t > u) = \begin{cases} 1, & R_t > u, \\ 0, & \text{otherwise} \end{cases} \tag{11}$$

For a higher level $x > u$, the conditional probability of exceedance is:

$$P(R_t > x) = P(R_t > u)\left(1 + \frac{\xi(x-u)}{\sigma}\right)^{-1/\xi}, \quad x > u \tag{12}$$

The corresponding return period is:

$$T = \frac{1}{P(R_t > x)} \tag{13}$$

where T represents the average interval between exceedances. For the non-stationary model, return levels were estimated under three covariate scenarios (minimum, mean, and maximum), where the mean scenario corresponds to all covariates fixed at their sample mean values, the minimum scenario to their joint minimum values, and the maximum scenario to their joint maximum values. Covariates were standardized using the same mean and standard deviation as during model fitting. The resulting shape and scale parameters, along with the exceedance rate, were used to calculate exceedance probabilities and return periods.

4. Results and Discussion

4.1. Estimation of Impervious Surface Percentage

The impervious surface percentage for 1960-1974 was estimated using data from 1975-2024. A time series plot visualized the growth trend. The observed trend was nonlinear, characterized by slow growth prior to the mid-1990s and a marked acceleration thereafter. As shown in Table 1, the logistic model yielded a substantially lower AIC value than the linear model, indicating superior performance in capturing the nonlinear growth of impervious surfaces. Consequently, the logistic model was selected to harmonize the impervious surface percentage series over the full 1960–2024 period for consistency with other datasets.

Table 1. *Comparison of linear and logistic growth models fitted to impervious surface percentage data (1975–2024) for back-casting historical Impervious surface percentage trends, evaluated using the AIC.*

Model	AIC
Linear Model	-23.495
Logistic Model	-40.850

4.2. Rainfall Data Stitching, Validation, and Trend Testing

To assess consistency between TerraClimate and CHIRPS datasets over 1981–2024, monthly differences were examined. The Shapiro-Wilk test indicated non-normality (Table 2), confirmed visually with a histogram (Figure 1).

Table 2. *Shapiro–Wilk normality test for monthly rainfall differences (1981–2024) between the TerraClimate and CHIRPS datasets. The p-value (< 0.05) indicates a significant deviation from normality.*

Test	W Statistic	p-value
Shapiro–Wilk Test	0.88727	$< 2.2 \times 10^{-16}$

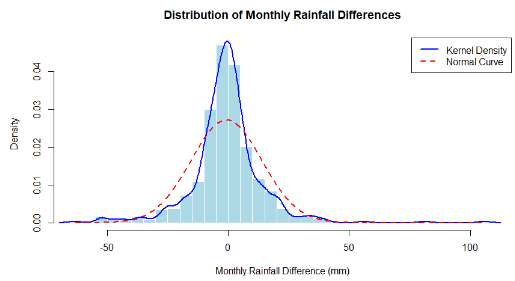

Figure 1. *Histogram of monthly rainfall differences (1981–2024) between the TerraClimate and CHIRPS datasets. The distribution shows a clear departure from normality, confirming the results of the Shapiro–Wilk test (Table 2).*

The non-parametric Wilcoxon signed-rank test indicated no significant median difference, while Spearman correlation (0.92) confirmed strong association (Table 3).

Table 3. *Results of the Wilcoxon signed-rank test and Spearman correlation analysis comparing TerraClimate and CHIRPS monthly rainfall data (1981–2024). The Wilcoxon test assesses whether the median difference between datasets differs from zero, while Spearman correlation quantifies the strength of the monotonic relationship between the datasets.*

Test / Correlation Type	Statistic / Coefficient	p-value
Wilcoxon Signed-Rank Test	63,856	0.08865
Spearman correlation	0.92	—

Visual comparisons using scatter plots, time series, boxplots, and density plots showed strong agreement (Figure 2).

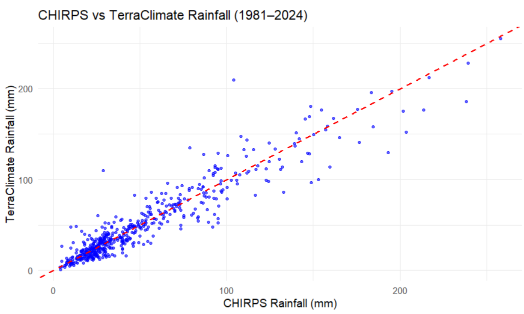

(a) *Scatter plot.*

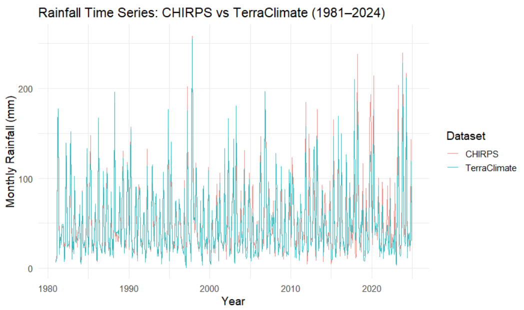

(b) *Time series overlay.*

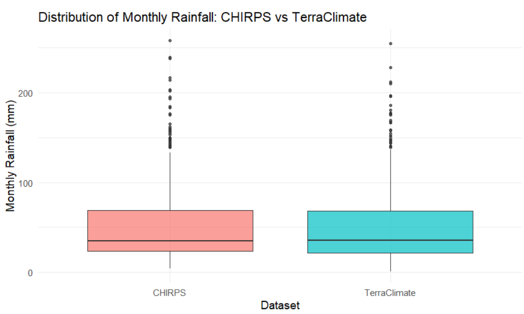

(c) *Boxplot.*

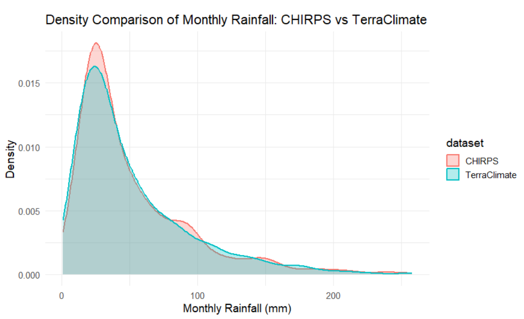

(d) *Density plots.*

Figure 2. *Visual comparison of TerraClimate and CHIRPS datasets (1981–2024). Subfigures show agreement across scatter, time series, boxplot, and density plots.*

A KS test confirmed no significant difference in distributions, supporting the merging of datasets (Table 4).

Table 4. *KS test comparing TerraClimate and CHIRPS monthly rainfall distributions (1981–2024). The KS test evaluates whether the two datasets originate from the same distribution.*

Test	D Statistic	p-value
Kolmogorov–Smirnov Test	0.064394	0.2237

The MK test indicated that rainfall remained statistically stable ($\tau = 0.0018$, $p = 0.94$), while SST and ISP showed strong upward trends ($\tau = 0.218$ and 0.961, $p < 0.001$). AMC exhibited no notable trend ($\tau = 0.0214$, $p = 0.372$). These results align with global observations, such as the 2024 record-high African SSTs reported by the [34], and reflect ongoing urbanization increasing impervious surfaces. Seasonal trends for MAM and OND showed no significant trends (MAM: $\tau = -0.042$, $p = 0.622$; OND: $\tau = 0.059$, $p = 0.493$).

Table 5. *MK trend test results for rainfall and selected covariates over the study period. Kendall's τ indicates the direction and strength of monotonic trends, while the associated two-sided p-values assess their statistical significance.*

Variable	Kendall's τ	2-sided p-value
Rainfall (mm)	0.00179	0.94056
SST ($^\circ C$)	0.218	$< 2.22 \times 10^{-16}$
ISP (%)	0.961	$< 2.22 \times 10^{-16}$
ATM (mm)	0.0214	0.37154

While rainfall itself shows no long-term trend, the upward trends in SST and ISP support using a non-stationary GPD, allowing scale and shape parameters to reflect evolving environmental conditions. The lack of seasonal rainfall trends justifies a constant threshold in extreme value analysis.

4.3. The Generalized Pareto Distribution

4.3.1. Threshold Selection for the Stationary GPD

Stationary GPD models were fitted at the 0.90, 0.91, 0.92, 0.93, 0.94, and 0.95 quantiles. The stability of the shape parameter (ξ) across thresholds was examined, with preference for quantiles where ξ fluctuated minimally, reflecting consistent tail behavior.

Shape and scale parameters across thresholds are given in Table 6; ξ is stable between 0.90–0.93. The scale parameter (σ) gradually decreased with increasing thresholds.

Table 6. *Stationary GPD scale and shape parameter values across candidate threshold quantiles.*

Threshold	Scale (σ)	Shape (ξ)
0.90	48.11	–0.118
0.91	46.35	–0.105
0.92	45.15	–0.099
0.93	45.35	–0.108
0.94	36.95	–0.018
0.95	36.06	0.000

Visual assessment of the P-P, Q-Q and return level plots showed good fit across the 0.90-0.93 range. The 0.92 quantile was selected as it lies within the stable region of both ξ and σ, balancing a sufficiently high threshold for extreme events while retaining enough exceedances for robust estimation.

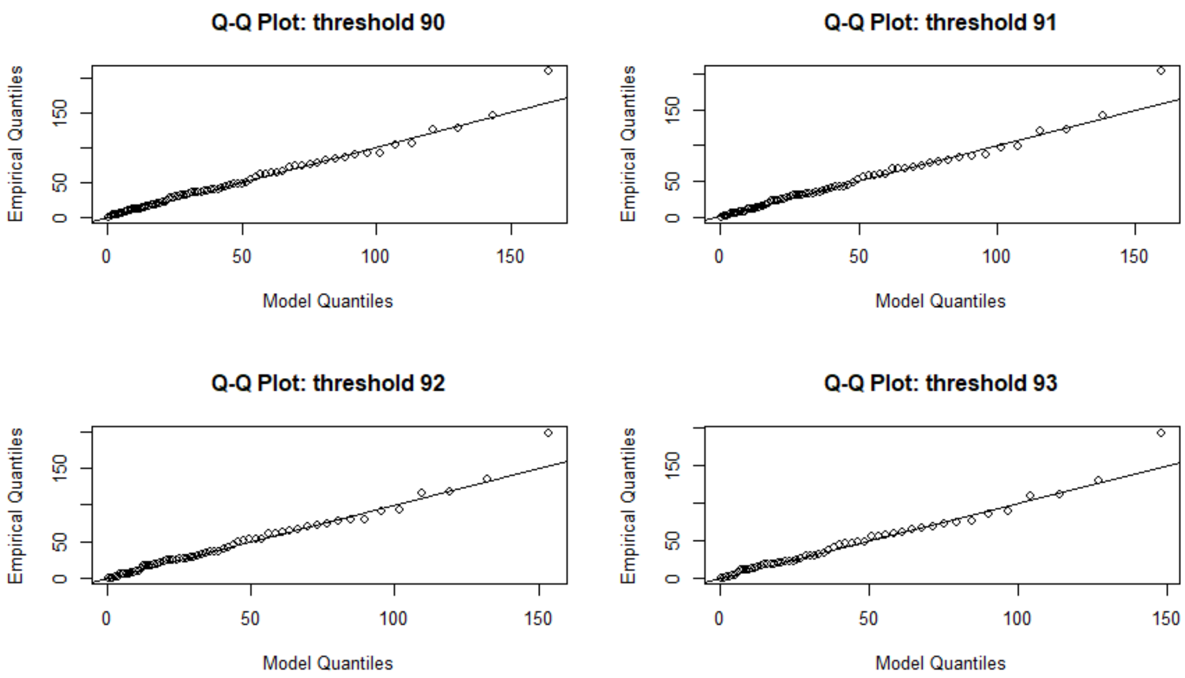

Figure 3. *Q-Q plots comparing empirical exceedances with stationary GPD model quantiles for thresholds 0.90-0.93.*

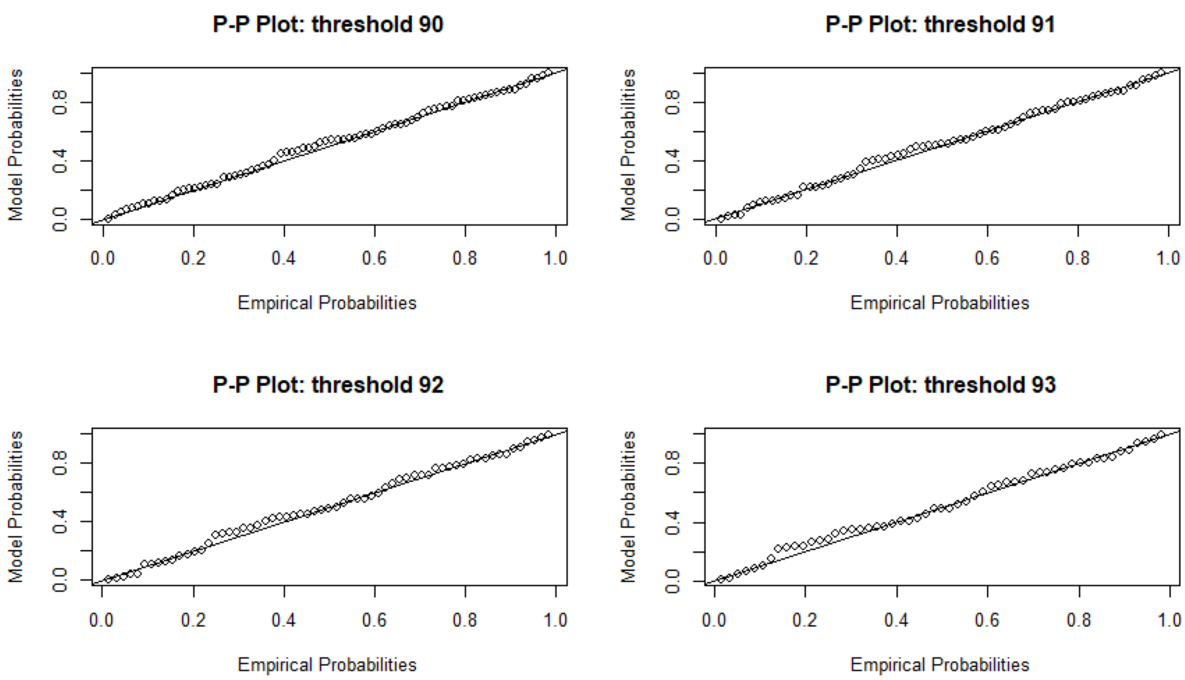

Figure 4. *P-P plots comparing empirical exceedance probabilities with those implied by stationary GPD models fitted at threshold quantiles 0.90-0.93.*

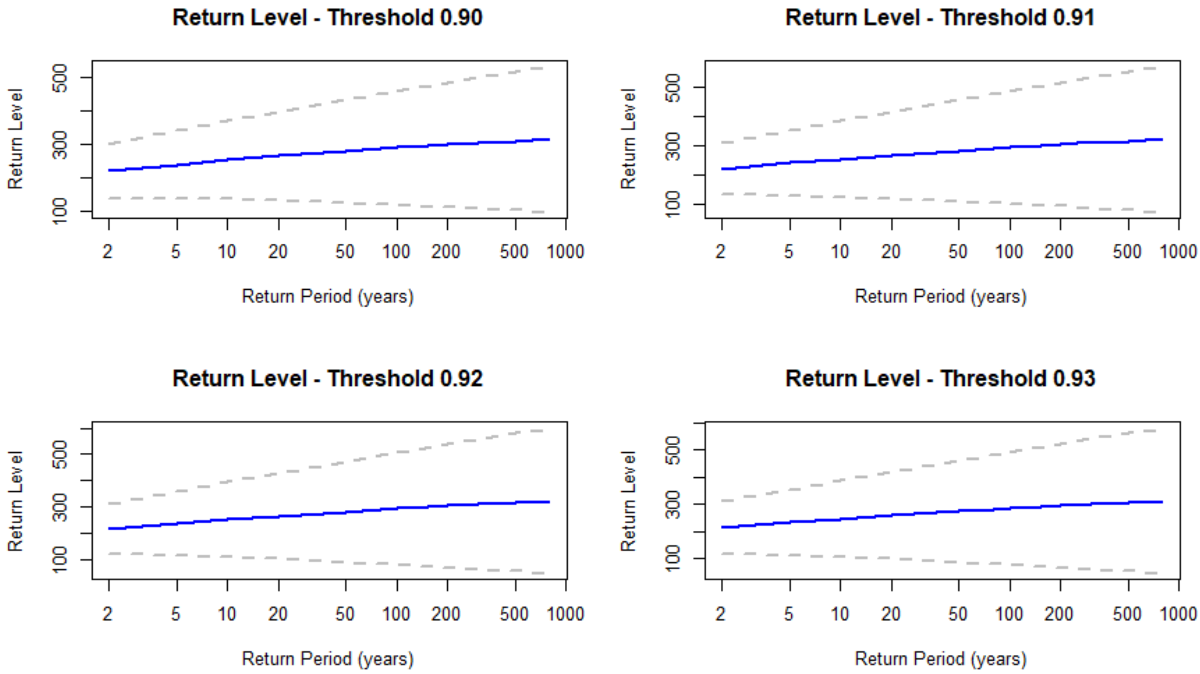

Figure 5. Return level plots for stationary GPD models fitted at threshold quantiles 0.90-0.93.

4.3.2. Stationary GPD Model

The scale and shape parameters were estimated using MLE with 95% confidence intervals. The tail appears light, with CIs including zero, motivating exploration of a non-stationary GPD (Table 7). Covariance between the scale and shape parameters, as well as the AIC and BIC values, indicate reasonable model fit.

Table 7. Maximum likelihood parameter estimates, associated uncertainty measures, and goodness-of-fit statistics for the stationary GPD fitted to exceedances above the 0.92 quantile threshold.

Feature	Estimate	SE	95% CI (Wald)
Scale (σ)	45.15	7.47	(30.51, 59.79)
Shape (ξ)	-0.099	0.108	(-0.310, 0.112)
Covariance (scale, shape)		-0.589	
Var(scale)		55.82	
Var(shape)		0.0116	
AIC		597.39	
BIC		601.68	
Neg. log-likelihood		296.69	

4.3.3. Model Fit Assessment

Model adequacy was evaluated using Q-Q and P-P plots, as well as a one-sample KS test. Figures 3 and 4 show that the empirical quantiles and probabilities closely follow the theoretical reference lines, indicating a good fit. The KS test further supports this, with $D = 0.0722$ and $p = 0.8741$, showing that the sample distribution closely matches the fitted GPD.

4.4. Assessment of EVT Assumptions

The independence of threshold exceedances was evaluated using the autocorrelation function and confirmed with the Runs test (p = 0.8973). Both tests showed no significant serial dependence, so declustering was not required. Examination of the time series of exceedances showed only a mild upward tendency (but it was not strong enough to suggest a systematic trend), suggesting that the exceedances were approximately identically distributed over time. Finally, the exceedances exhibited a right-skewed distribution with a pronounced upper tail, confirming that the tail behavior assumption for EVT was satisfied. Together, these results indicate that the data met the key assumptions required for Peaks-Over-Threshold modeling.

4.5. Non-Stationary GPD

4.5.1. Model Specification

Unlike the stationary model where scale and shape parameters are constant, the non-stationary GPD allowed both parameters to vary with covariates. Models were evaluated using negative log-likelihood (NegLogLik), AIC, and BIC.

Table 8. *Top 5 non-stationary GPD models fitted to threshold exceedances, ranked by AIC. Each row shows the covariates used for the scale (σ) and shape (ξ) parameters, along with the corresponding NegLogLik, AIC, and BIC values.*

σ	ξ	NegLogLik	AIC	BIC
z_2	z_1	284.671	577.341	585.914
$z_1 + z_2$	z_1	284.085	578.170	588.886
$z_1 + z_2$	z_3	286.046	582.092	592.807
$z_1 + z_2$	z_2	286.193	582.385	593.101
z_2	z_3	289.628	587.255	595.828

The chosen non-stationary mode had scale depending on z_2 and z_1:

$$\log(\sigma) = \sigma_0 + \sigma_1 z_2, \qquad \xi = \xi_0 + \xi_1 z_1$$

MLEs: $\sigma_0 = 60.51$ $(SE = 9.87)$, $\sigma_1 = 17.59$ $(SE = 3.60)$, $\xi_0 = -0.556$ $(SE = 0.139)$ and $\xi_1 = -0.207$ $(SE = 0.043)$.

It achieved the lowest NegLogLik (284.671), AIC (577.341), and BIC (585.914).

4.5.2. Selected Covariates

Impervious Surface Percentage (z_3) was initially included as a proxy for land-use change and was evaluated alongside the atmospheric covariates (z_1 and z_2) within the non-stationary GPD framework, allowing covariates to influence both the scale and shape parameters. Several model formulations incorporating z_3 were fitted and compared using the NegLogLik, AIC, and BIC.

Across all tested configurations, models including z_3 consistently underperformed relative to models that included only atmospheric covariates. As shown in Table 8, the best-performing model incorporating z_3 (with $z_1 + z_2$ affecting the scale and z_3 affecting the shape) achieved a NegLogLik of 286.046, AIC of 582.092, and BIC of 592.807. In contrast, the selected model without z_3 attained lower values of 284.671 (NegLogLik), 577.341 (AIC), and 585.914 (BIC). Consequently, z_3 was excluded from the final selected model.

4.5.3. Fit Assessment

Q-Q plot confirms good fit.

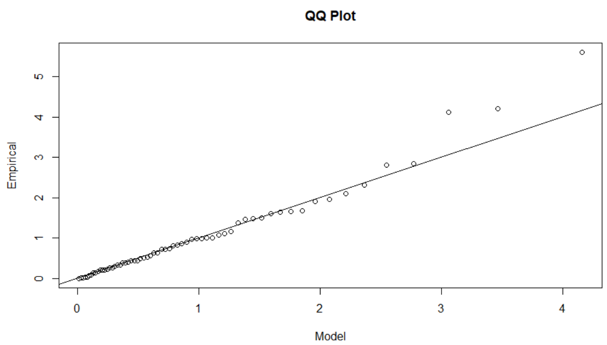

Figure 6. *Q-Q plot for the selected non-stationary GPD model, illustrating the agreement between observed exceedances and the fitted distribution.*

P-P plot confirms good fit.

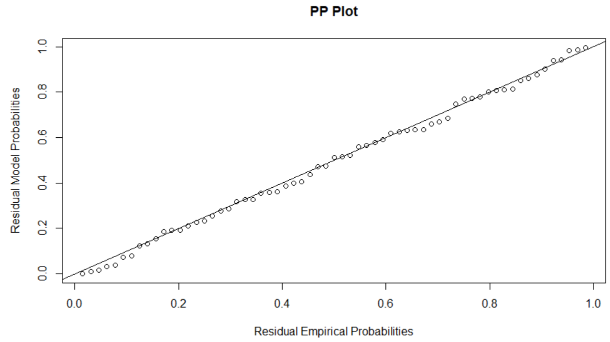

Figure 7. *P-P plot for the selected non-stationary GPD model, illustrating the agreement between observed exceedance probabilities and the fitted distribution.*

4.6. Model Comparison and Evaluation

This section compares the predictive performance of the stationary and non-stationary GPD models using historical rainfall data. The focus was on identifying which model better represents extreme rainfall events.

Stationary GPD: NegLogLik = 296.70, AIC = 597.39, BIC = 601.68

Non-stationary GPD: NegLogLik = 284.67, AIC = 577.34, BIC = 585.91

The LRT statistic = 24.05 and p-value < 0.05 confirmed that including covariates in the non-stationary model significantly improved fit ($p < 0.05$), justifying the adoption of the non-stationary GPD for modeling extreme rainfall events.

4.7. Return Levels for the Best Model

In the selected non-stationary model, both the scale and shape parameters were allowed to vary as functions of the covariates. The resulting average return levels are presented in Table 9

Table 9. *Estimated return levels from the final selected non-stationary GPD model, with scale (σ) and shape (ξ) parameters varying with covariates.*

10-year level	20-year level	50-year level	100-year level
238.55	239.77	241.08	242.90

These values indicate that, on average 10–100 year return levels ranged from 238.6 to 242.9 mm. The relatively small increase between the 10-year and 100-year return levels suggested bounded-tail behavior, which was consistent with the negative shape parameter estimated from the chosen non-stationary model.

4.8. Risk Estimates

Risk estimates and corresponding return periods were calculated for rainfall amounts of 150 mm, 200 mm, and 250 mm. Because the non-stationary GPD model allowed the shape parameter to vary with covariates, the implied upper bound for extreme rainfall differed across scenarios. For example, under the minimum, mean, and maximum covariate conditions, the upper bounds were approximately 389 mm, 232 mm, and 245 mm, respectively.

Consequently, rainfall exceeding 250 mm was possible only under the minimum scenario ($max \approx 389mm$). For the mean and maximum scenarios, 250 mm exceeded the upper bound, so the probability of observing such an extreme was very small (almost zero), resulting in an undefined return period.

Overall, probabilities of extreme rainfall (150 - 250 mm) were low under typical and dry covariate conditions, but increase under the wettest scenarios. For example, under maximum covariates, the probability of exceeding 150 mm was 0.0637 ($returnperiod \approx 16months$), compared to 0.0426 and 0.0291 for the mean and minimum scenarios, respectively. This highlights the strong influence of covariates on extreme rainfall risk.

Table 10. *Estimated probabilities and return periods for extreme rainfall under minimum, mean, and maximum covariate scenarios, based on the selected final non-stationary GPD model.*

Rainfall (mm)	Scenario	Probability	Return Period
150	Mean	0.04263788	23.45332
200	Mean	0.02572694	38.86975
250	Mean	0.00000000	N/A
150	Min	0.02914451	34.31178
200	Min	0.02665735	37.51311
250	Min	0.02548050	39.24569
150	Max	0.06368212	15.70299
200	Max	0.04176498	23.94350
250	Max	0.00000000	N/A

5. Conclusion

5.1. Summary of the Findings

This study compared stationary and non-stationary extreme value models for rainfall extremes in Kenya using a POT framework. Threshold diagnostics showed no persistent long-term trend in the rainfall series, supporting the use of a constant threshold, consistent with previous studies in East Africa [16,30].

The first objective involved extending the POT framework by incorporating climate covariates. Non-stationarity was introduced by allowing the scale and shape parameters to vary with the climate related covariates. Several alternative specifications were explored, with unstable or non-convergent models excluded prior to selection. The final model was chosen based on information criteria (NegLogLik, AIC, and BIC) among stable and interpretable formulations. The selected non-stationary GPD model retained only AMC and SST as covariates influencing the scale and shape parameters. This indicates that, at the spatial and temporal scale considered in this study, large-scale atmospheric conditions dominate the behavior of extreme rainfall, while land-surface characteristics such as imperviousness do not provide additional explanatory power for the statistical tail behavior once atmospheric drivers are accounted for.

These findings do not imply that impervious surfaces are unimportant for hydrological impacts. Rather, they suggest that ISP primarily affects runoff generation and flood response processes, whereas extreme rainfall magnitudes are governed predominantly by synoptic-scale circulation and moisture availability.

The second and third objectives addressed parameter estimation and model comparison. The selected threshold corresponds to the 0.92 quantile (122.99 mm), which represents rainfall amounts capable of generating substantial surface runoff and flooding impacts in the study area. Events of this magnitude are relatively rare and mark a transition from ordinary rainfall to hydrologically significant extremes. Although the threshold was first identified using statistical diagnostics and parameter stability, it also aligns well with physically meaningful high-impact rainfall levels. Sensitivity checks across nearby thresholds (0.90-0.93) showed comparable model behavior, indicating robustness to the exact choice. Overall, the 0.92 quantile offers a practical balance between physical interpretability, statistical reliability, and adequate data support. Across all diagnostics-AIC, BIC, NegLogLik values, and likelihood ratio testing- the non-stationary GPD consistently outperformed the stationary model. Incorporating covariates captured climate-driven variability in extreme rainfall more realistically than fixed-parameter models, aligning with findings by [31].

Return level analysis showed only modest increases in rainfall magnitude with longer return periods, indicating saturation rather than unbounded growth. This bounded-tail behavior has important implications for flood risk assessment and infrastructure design. Risk estimates further revealed strong sensitivity to covariate states, with exceedance probabilities increasing substantially under extreme climatic conditions.

The small difference between 10 years and 100 years does not imply a physical limit on rainfall. It rather indicated that under observed extreme rainfall events and climate conditions, increasingly rare events are not substantially larger than already extreme rainfall. Such behavior is physically plausible given constraints on atmospheric moisture and storm duration. The implied upper bound is therefore model-conditional and should not be interpreted as an absolute climatic maximum.

Overall, the results demonstrate that rainfall extremes in Kenya are better characterized using a non-stationary framework that explicitly accounts for climate drivers, highlighting the limitations of stationary assumptions for risk-based decision-making.

5.2. Conclusions

Based on the results of this study, the following conclusions are drawn:

1. The stationary GPD model adequately describes rainfall exceedances but does not capture the influence of climate drivers.

2. Incorporating AMC and SST as covariates within a non-stationary GPD framework significantly improves model performance, as confirmed by the likelihood ratio test ($p < 0.05$).
3. Return level estimates increased only slightly with longer return periods (from 238.55 mm for the 10-year event to 242.90 mm for the 100-year event), indicating a saturation effect. This does not imply a strict physical limit on rainfall, but rather indicates that, under observed extreme rainfall and climate conditions, increasingly rare events are not substantially larger than already extreme storms.
4. Risk analysis revealed strong sensitivity to climatic conditions: exceedance probabilities were low under mean covariate values but increased markedly under maximum covariate states, leading to shorter return periods.

The use of national-scale rainfall data provided a broad baseline assessment relevant for disaster risk reduction, adaptation planning, and climate policy in Kenya. However, Kenya's rainfall regimes are highly heterogeneous, and national-scale analyses may mask localized trends present in more homogeneous sub-regions. Regional-scale studies are therefore needed to complement these findings and support location-specific infrastructure and risk management decisions.

Overall, this study demonstrates the value of non-stationary extreme value modeling for improving the understanding of rainfall extremes under changing climatic conditions. By incorporating sea surface temperature and atmospheric moisture into the modeling framework, the analysis offers a more realistic representation of environmental variability and provides a strong methodological foundation for future applications in Kenya and other regions.

5.3. Recommendations

Given the strong influence of atmospheric moisture content and sea surface temperature on extreme rainfall, policymakers, urban planners, and water resource managers should avoid relying solely on historical rainfall records and instead incorporate relevant climate drivers into risk assessments and infrastructure design.

5.4. Areas of Further Research

1. Future studies should consider a broader range of climatic and environmental covariates to better capture their influence on rainfall extremes.
2. Bayesian estimation approach and other estimation methods could be explored as alternatives to MLE, particularly in cases with limited exceedance data, to improve parameter stability.
3. Extending the analysis to regional or sub-national scales would provide deeper insight into spatial variability in extreme rainfall and support more targeted flood risk management strategies.

ORCID

0009-0005-8267-5785 (Simion, Mike Mbumbu)
0000-0003-0268-2968 (Anthony Waititu)
0009-0003-9963-4977 (Herbert Imboga)
0009-0005-9570-9112 (Susan Mwelu)

Abbreviations

GPD	Generalized Pareto Distribution
POT	Peaks-Over-Threshold
SST	Sea Surface Temperature
AMC	Atmospheric Moisture Content
ISP	Impervious Surface Percentage
BM	Block Maxima
GEV	Generalized Extreme Value
EVT	Extreme Value Theory
MLE	Maximum Likelihood Estimation
AIC	Akaike Information Criterion
BIC	Bayesian Information Criterion
CHIRPS	Climate Hazards Group InfraRed Precipitation with Station data
NOAA	National Oceanic and Atmospheric Administration
ERA5	ECMWF Reanalysis 5th Generation
ENSO	El Niño-Southern Oscillation
KS	Kolmogorov-Smirnov (test)
QGIS	Quantum Geographic Information System.
GHSL	Global Human Settlement Layer
MK	Mann-Kendall
MAM	March-May (rain)
OND	October-December (rain)
Q-Q	Quantile-Quantile (plot)
P-P	Probability-Probability (plot)
PDF	Probability Density Function
CDF	Cumulative Distribution Function
LRT	Likelihood Ratio Test
NegLogLik	Negative Log-Likelihood

Acknowledgments

The author sincerely thanks Professor Anthony Waititu, Dr. Herbert Imboga, and Dr. Susan Mwelu for their invaluable guidance, constructive feedback, and continuous support throughout this research. Appreciation is also extended to colleagues and friends for their encouragement. The author gratefully acknowledges the organizations and institutions that made the data used in this study available.

Author Contributions

Simion Mike Mbumbu: Conceptualization, Data curation, Formal analysis, Investigation, Methodology, Project administration, Software, Validation, Visualization, Writing - original draft, Writing - review & editing.

Anthony Waititu: Formal analysis, Investigation, Data curation, Methodology, Software, Supervision, Validation, Visualization.

Herbert Imboga: Conceptualization, Investigation, Data curation, Methodology, Resources, Supervision, Writing - review & editing.

Susan Mwelu: Conceptualization, Supervision, Validation, Writing - review & editing

Conflicts of Interest

The authors declare that there are no conflicts of interest related to this study.

References

[1] Assessment Capacities Project. (2024). Kenya: Heavy rainfall and floods. ACAPS. https://www.acaps.org/fileadmin/Data_Product/Main_media/20240514_ACAPS_Briefing_note_Kenya_Floods.pdf

[2] Acero, F. J., Garcia, J. A., and Gallego, M. C. (2011). Peaks-over-Threshold Study of Trends in Extreme Rainfall over the Iberian Peninsula. Journal of Climate, 24(4), 1089-1105. https://doi.org/10.1175/2010JCLI3627.1

[3] Africa Center for Strategic Studies. (2024). Record Levels of Flooding in Africa Compounds Stress on Fragile Countries. https://africacenter.org/spotlight/record-levels-of-flooding-in-africa-compounds-stress-on-fragile-countries/

[4] Alsilibe, F., Bene, K., Bilal, G., Alghafli, K., and Shi, X. (2023). Accuracy Assessment and Validation of Multi-Source CHIRPS Precipitation Estimates for Water Resource Management in the Barada Basin, Syria. Remote Sensing, 15(7), 1778. https://doi.org/10.3390/rs15071778

[5] Arregoces, H. A., Rojano, R., and Pérez, J. (2023). Validation of the CHIRPS dataset in a coastal region with extensive plains and complex topography. Case Studies in Chemical and Environmental Engineering, 8, 100452. https://doi.org/10.1016/j.cscee.2023.100452

[6] Arshad, A., Mirchi, A., He, C., Shah, A. A., and AghaKouchak, A. (2025). Anthropogenic and climatic drivers of the 2022 mega-flood in Pakistan. npj Natural Hazards, 2(57). https://doi.org/10.1038/s44304-025-00109-z

[7] Bagiliko, J., Stern, D., Ndanguza, D., and Torgbor, F. F. (2025). Validation of satellite and reanalysis rainfall products against rain gauge observations in Ghana and Zambia. Theoretical and Applied Climatology, 156, 241. https://doi.org/10.48550/arXiv.2501.14829

[8] Balkema, A. A., and de Haan, L. (1974). Residual Life Time at Great Age. The Annals of Probability, 2(5), 792-804. https://doi.org/10.1214/aop/1176996548

[9] Begueria, S., Angulo-Martínez, M., Vicente-Serrano, S. M., López-Moreno, J. I., and El-Kenawy, A. (2011). Assessing trends in extreme precipitation events intensity and magnitude using non-stationary peaks-over-threshold analysis: a case study in northeast Spain from 1930 to 2006. International Journal of Climatology, 31(14), 2102-2114. http://dx.doi.org/10.1002/joc.2218

[10] Blenkinsop, S., Fowler, H. J., Barbero, R., et al. (2018). The INTENSE project: using observations and models to understand the past, present and future of sub-daily rainfall extremes. Advances in Science and Research, 15, 117-126. https://doi.org/10.5194/asr-15-117-2018

[11] Cattani, E., Merino, A., Guijarro, J. A., and Levizzani, V. (2018). East Africa Rainfall Trends and Variability 1983-2015 Using Three Long-Term Satellite Products. Remote Sensing, 10(6), 931. https://www.mdpi.com/2072-4292/10/6/931

[12] Coles, S. (2001). An Introduction to Statistical Modeling of Extreme Values. London: Springer. https://doi.org/10.1007/978-1-4471-3675-0

[13] Dey, A. K., and Patwary, M. S. A. (2025). Utilizing non-stationary extreme value model to quantify extreme rainfall in two major cities in Bangladesh. Stochastic Environmental Research and Risk Assessment, 39(6), 2281-2296 https://doi.org/10.1007/s00477-025-02969-3

[14] Du, H., Tan, M. L., Zhang, F., Chun, K. P., Li, L., and Kabir, M. H. (2024). Evaluating the effectiveness of CHIRPS data for hydroclimatic studies. Theoretical and Applied Climatology, 155, 1519-1539. https://doi.org/10.1007/s00704-023-04721-9

[15] Economy Insights. (2025). The World's Costliest Floods: A Look at the Flood Disasters With the Highest Economic Losses. https://www.economyinsights.com/p/the-worlds-costliest-floods

[16] Gebrechorkos, S. H., Hulsmann , S., and Bernhofer, C. (2019). Long-term trends in rainfall and temperature using high-resolution climate datasets in East Africa. Scientific Reports 9, 11376. https://www.nature.com/articles/s41598-019-47933-8

[17] Ghalavand, M. R., Farajzadeh, M., and Ghavidel Rahimi, Y. (2025). Modeling return levels of non-stationary rainfall extremes due to climate change. Atmosphere 16(2), 136. https://doi.org/10.3390/atmos16020136

[18] Gumbel, E. J. (1958). Statistics of Extremes. Columbia University Press. https://doi.org/10.7312/gumb92958

[19] Hao, W., Shao, Q., Hao, Z., Ju, Q., Baima, W., and Zhang, D. (2019). Non-stationary modelling of extreme precipitation by climate indices during rainy season in Hanjiang River Basin, China. International Journal of Climatology 39(7), https://doi.org/10.1002/joc.6065

[20] Katz, R. W., Parlange, M. B., and Naveau, P. (2002). Statistics of extremes in hydrology. Advances in Water Resources 25(8-12), 1287-1304. https://doi.org/10.1016/S0309-1708(02)00056-8

[21] Katz, R. W. (2013). Statistical methods for nonstationary extremes. In Extremes in a Changing Climate: Detection, Analysis & Uncertainty, A. AghaKouchak, D. Easterling, K. Hsu, S. Schubert, and S. Sorooshian, Eds., Dordrecht, Netherlands: Springer Netherlands, pp. 15-37. https://doi.org/10.1007/978-94-007-4479-0_2

[22] Kyojo, E. A., Mirau, S. S., Osima, S. E., and Masanja, V. G. (2024). Frequentist and Bayesian Approaches in Modeling and Prediction of Extreme Rainfall Series: A Case Study from Southern Highlands Region of Tanzania. Advances in Meteorology, 2024, 1-14. https://doi.org/10.1155/2024/8533930

[23] Maposa, D., Cochran, J. J., and Lesaoana, M. (2016). Modelling non-stationary annual maximum flood heights in the lower Limpopo River basin of Mozambique. Journal of the South African Statistical Association, 50(1), 55-68. https://doi.org/10.4102/jamba.v8i1.185

[24] Masingi, V. N. and Maposa, D. (2021). Modelling Long-Term Monthly Rainfall Variability in Selected Provinces of South Africa: Trend and Extreme Value Analysis Approaches. Hydrology, 8(2), 70. https://doi.org/10.3390/hydrology8020070

[25] Mulwa, C. M., Imboga, H., and Mwelu, S. (2026). Modelling the Dependence Between Drought and Heatwave Extremes in Kenya Using an Integrated EVT-Copula-XGBoost Framework. American Journal of Mathematical and Computer Modelling, 11(1), 1-12. https://doi.org/10.11648/j.ajmcm.20261101.11

[26] Mwenda, N. D., Odira, P. M. A., and Nyanchaga, E. N. (2019). Trend Detection in Precipitation and River Discharge to Assess Climate Change in the Upper Tana Basin. International Journal of Innovative Studies in Sciences and Engineering Technology (IJISSET), 5(6), 18-26. https://ijisset.org/storage/Volume5/Issue6/IJISSET-050610.pdf

[27] Onwuegbuche, F. C., Kenyatta, A. B., Affognon, S. B., Enock, E. P., and Akinade, M. O. (2019). Application of Extreme Value Theory in Predicting Climate Change Induced Extreme Rainfall in Kenya. International Journal of Statistics and Probability, 8(4), 85-96. https://doi.org/10.5539/ijsp.v8n4p85

[28] Pen, S., Rad, S., Ban, L., Brang, S., Nuth, P., and Liao, L. (2024). An Analysis of Extreme Rainfall Events in Cambodia. Atmosphere, 15(8), 1017. https://doi.org/10.3390/atmos15081017

[29] Pickands, J. (1975). Statistical Inference Using Extreme Order Statistics. The Annals of Statistics, 3(1), 119-131. https://doi.org/10.1214/aos/1176343003

[30] Rodhe, H. and Virji, H. (1976). Trends and Periodicities in East African Rainfall Data. Monthly Weather Review, 104(3), 307-315. https://doi.org/10.1175/1520-0493(1976)104%3C0307:TAPIEA%3E2.0.CO;2

[31] Roth, M., Buishand, T. A., Jongbloed, G., Klein Tank, A. M. G., and van Zanten, J. H. (2012). A regional peaks-over-threshold model in a nonstationary climate. Water Resources Research, 48(11), W11533. https://doi.org/10.1029/2012WR012214

[32] Wasko, C., Nathan, R., Stein, L., and O'Shea, D. (2021). Evidence of shorter, more extreme rainfalls and increased flood variability under climate change. Journal of Hydrology, 603, 126994. https://doi.org/10.1016/j.jhydrol.2021.126994

[33] Wing, O. E. J., Bates, P. D., Quinn, N. D., Savage, J. T. S., Uhe, P. F., Cooper, A., Collings, T. P., Addor, N., Lord, N. S., Hatchard, S., Hoch, J. M., Bates, J., Probyn, I., Himsworth, S., Rodríguez González, J., Brine, M. P., Wilkinson, H., Sampson, C. C., Smith, A. M., Neal, J. C., and Haigh, I. D. (2024). A 30 m Global Flood Inundation Model for Any Climate Scenario. Water Resources Research. https://doi.org/10.1029/2023WR036460

[34] World Meteorological Organization. (2025). Extreme weather and climate change impacts hit Africa hard (WMO). https://wmo.int/news/media-centre/extreme-weather-and-climate-change-impacts-hit-africa-hard

[35] Zhang, W., Sun, L., Zhang, X., Hegerl, G. C., and Zwiers, F. W. (2024). Anthropogenic amplification of precipitation variability over the past century. Science 385(6652), 457–462. https://www.science.org/doi/10.1126/science.adp0212